**Xianghong Xu**[1]
State Key Laboratory of Nonlinear Mechanics,
Institute of Mechanics,
Chinese Academy of Sciences,
No. 15 Beisihuanxi Road,
Beijing 100190, China
e-mail: xxh@lnm.imech.ac.cn

**Zhongkang Lin**
State Key Laboratory of Nonlinear Mechanics,
Institute of Mechanics,
Chinese Academy of Sciences,
No. 15 Beisihuanxi Road,
Beijing 100190, China

**Shilong Sheng**
State Key Laboratory of Nonlinear Mechanics,
Institute of Mechanics,
Chinese Academy of Sciences,
No. 15 Beisihuanxi Road,
Beijing 100190, China

**Wenjun Yuan**
State Key Laboratory of Nonlinear Mechanics,
Institute of Mechanics,
Chinese Academy of Sciences,
No. 15 Beisihuanxi Road,
Beijing 100190, China

# Evolution Mechanisms of Thermal Shock Cracks in Ceramic Sheet

*Knowledge of crack initiation, propagation, and corresponding thermal shock failure evolution is prerequisite for effective maintenance of civil engineering so as to avoid disaster. Experimental analysis of the cracking in the ceramic sheets subsequent to water quenching has been conducted. Based on statistical mesoscopic damage mechanics, it was revealed that there are four stages in the process of thermal shock evolution of ceramics subjected to water quenching. The multiple cracks interaction mechanism has been analyzed from the viewpoint of the evolution of the elastic strain energy and stress intensity factor.* [DOI: 10.1115/1.4033175]

*Keywords: ceramic, thermal shock, heterogeneity, crack interaction, depth grading*

## 1 Introduction

Ceramic has been widely used in industrial fields due to its intrinsically advanced thermal mechanical properties, anti-oxidation, and corrosion resistances. However, ceramics exhibit low resistance to fracture by thermal shock due to their brittleness, and often occur in cracking or worse, even a highly catastrophic failure. Therefore, thermal shock crack is one of the most primary reasons resulting in the failure in the ceramic structure, and thermal shock resistance undoubtedly restricts the ceramic engineering application in high-temperature environment. The study of the working mechanism of the crack growth induced by thermal shock not only could be able to assess the service life of the ceramic components to reduce the accident rate but also is helpful to design of ceramic with high thermal shock resistance.

The study on thermal shock damage problem of ceramic has been carried out since 1950s. In order to solve the above mentioned issues, a large number of research scholars had taken great effort on the aspects of theoretical model and analysis, experiment and numerical simulation, characterization, and evolution criterion. Lu and Fleck [1] analyzed the effect of different factors on thermal shock resistance of brittle solids based on a failure criterion. After that, the hot points of research have been turned to the evolution of the crack patterns, for instance, Bazant et al. [2] and Nemat-Nasser [3,4] studied the stability in crack growth according to parallel cycle way and proposed the instability criterion of the crack grading; Jagla [5] discussed the form and growth of cycle crack by the stress criterion and energy minimization; and Bahr et al. [6] derived the growth rule of the cycle thermal shock crack in the semi-infinite body. Bahr et al. [7,8] experimentally studied the evolution of crack patterns in the different thermal shock temperatures and carried out a qualitative analysis of multiple crack growth based on Griffith's criterion. Jenkins [9] and Jiang et al. [10] studied the evolution of spacing and depth of thermal shock crack using the energy minimization. Li et al. [11,12] simulated the extension of thermal shock crack by applying the nonlocal damage model. Sicsic and Bourdin [13,14] promoted the simulation for thermal shock crack in ceramic to 3D using the gradient-enhanced damage model and discussed the condition, under which the penetrating cracks are converted into the net cracks.

To date, the study on thermal shock damage in ceramic has been made the great progress. However, there are still several fundamental issues that need to be solved, such as ignoring the influence of the heterogeneity. Tang et al. [15–17] and Bai et al. [18–20] have proposed damage model studying concrete and rock fracture undergoing compression and other external loading. In this study, a theoretical model has been proposed for the thermal shock cracks growth of ceramic based on that given by Tang and Bai. The mechanism of the multiple thermal shock cracks evolution has been investigated and discussed.

## 2 Experimental Details

Commercially available $Al_2O_3$ powder (particle size 0.5 $\mu$m, purity 99.5%) was compressed into blocks at 20 MPa and subsequently sintered at 1650 °C for 2 hrs at normal pressure. The sintered bodies, with 4% porosity and 10 $\mu$m mean grain size, were cut into sheets with dimensions of 50 mm × 10 mm × 1 mm. The ceramic sheets were ground, polished, slightly chamfered, and then stacked as shown in Fig. 1 to prevent coolant from accessing the interior surfaces (50 mm × 10 mm). In such case, adiabatic boundary is satisfied on the left, right, and interior surfaces of the sheet, while convective heat transfer boundary is satisfied on the top and bottom surfaces.

The stacks were initially heated to a predetermined temperature in a muffle furnace (MF-0914P), kept for 20 min to reach thermal

[1]Corresponding author.

Contributed by the Applied Mechanics Division of ASME for publication in the Journal of Applied Mechanics. Manuscript received February 23, 2016; final manuscript received March 23, 2016; published online April 15, 2016. Editor: Yonggang Huang.

  

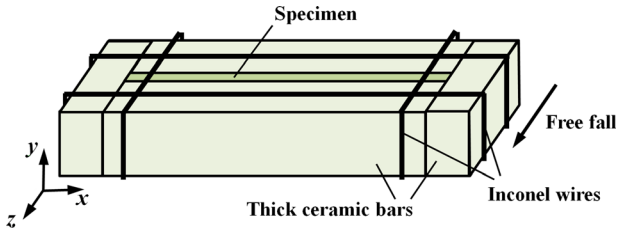


**Fig. 1 Schematic of bound ceramic sheet and free fall direction for thermal shock**

equilibrium, and then quenched in water at 17 °C. After drying, the quenched samples were immersed in dye and then wiped with absorbent cotton. The crack patterns of each specimen after quenching were thus distinguishable and were photographed by a digital scanner. Figure 2(*a*) shows the thermal shock cracks of three specimens quenched at 400 °C.

## 3 Numerical Simulations

**3.1 Theoretical Model.** A two-dimensional theoretical model is introduced to depict the above water quenching test of ceramic sheet. The specimen dimensions along $x$ and $y$ axes are $2L \times 2H$, where $L = 25$ mm and $H = 5$ mm, and both of them are far greater than that in the $z$ direction (Fig. 3).

The temperature field $T(x,y,t)$ is simplified as two-dimensional plane problem due to no heat exchange along the $z$ direction, and satisfies the Fourier heat equation as follows [1]:

$$\frac{\partial^2 T}{\partial x^2} + \frac{\partial^2 T}{\partial y^2} = \frac{1}{\kappa}\frac{\partial T}{\partial t}, \quad (|x| \le L, |y| \le H, t > 0) \tag{1}$$

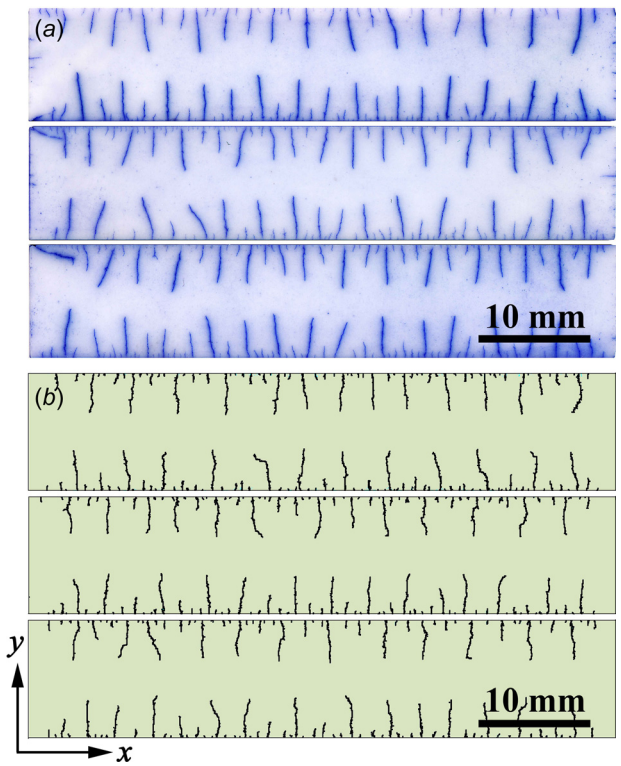


**Fig. 2 Thermal shock cracks on the interior surface of three ceramic sheets: (*a*) experimental results and (*b*) simulation results. The quench and water temperatures are 400 °C and 17 °C, respectively.**

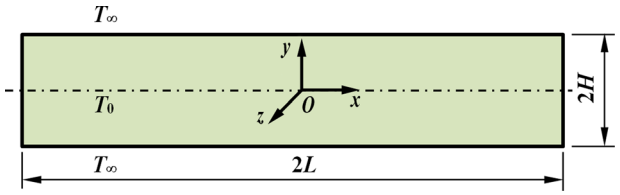


**Fig. 3 Theoretical model of ceramic sheet under water quenching**

where $\kappa = k/\rho c$ is the thermal diffusivity, $k$ is the thermal conductivity, $\rho$ is the density, and $c$ is the constant-pressure specific heat. At $t = 0$, the initial temperature of the sheet is $T_0$

$$T(x,y,t) = T_0, \quad (|x| \le L, |y| \le H, t = 0) \tag{2}$$

The top and bottom surfaces ($y = \pm H$) of the sheet are quenched in water at $T_\infty$ and can be expressed by the convection boundary condition, and the left and right surfaces are satisfied the adiabatic boundary condition

$$\left.\begin{aligned} k\frac{\partial T}{\partial y} &= \mp h(T - T_\infty), && (y = \pm H,\ t > 0) \\ \frac{\partial T}{\partial x} &= 0, && (x = \pm L,\ t > 0) \end{aligned}\right\} \tag{3}$$

where $h$ is the surface heat transfer coefficient.

The stress fields $\sigma_x(x,y,t)$, $\sigma_y(x,y,t)$, and $\tau_{xy}(x,y,t)$ are simplified as plane stress problem and satisfy the equilibrium equations as follows [9]:

$$\left.\begin{aligned} \frac{\partial \sigma_x}{\partial x} + \frac{\partial \tau_{xy}}{\partial y} &= 0 \\ \frac{\partial \tau_{xy}}{\partial x} + \frac{\partial \sigma_y}{\partial y} &= 0 \end{aligned}\right\} \tag{4}$$

The thermo-elastic constitutive relation is given as

$$\left.\begin{aligned} \varepsilon_x &= \frac{1}{E(i,t)}[\sigma_x - \nu\sigma_y] + \alpha(T - T_\infty) \\ \varepsilon_y &= \frac{1}{E(i,t)}[\sigma_y - \nu\sigma_x] + \alpha(T - T_\infty) \\ \gamma_{xy} &= \frac{2(1+\nu)}{E(i,t)}\tau_{xy} \end{aligned}\right\} \tag{5}$$

where $\varepsilon_x(x,y,t)$, $\varepsilon_y(x,y,t)$, and $\gamma_{xy}(x,y,t)$ are the strain fields. It was assumed that the specimen consists of a number of mesoscopic units, and each unit has the same Poisson's ratio $\nu$, thermal expansion coefficient $\alpha$, thermal conductivity $k$, constant-pressure specific heat $c$, and density $\rho$, but different mesoscopic mechanical properties. $E(i,t)$ represents the elastic modulus of the $i$th unit at the moment $t$, and the coordinate $(x,y)$ corresponds to a point within the $i$th element. Moreover, the thermal shock process is accompanied by the transformation from the heat energy to the elastic strain energy $U(t)$ which can be calculated by

$$U = \frac{1}{2}\int_{-L}^{L}\int_{-H}^{H}(\sigma_x\varepsilon_x + \sigma_y\varepsilon_y + \tau_{xy}\gamma_{xy})\mathrm{d}x\mathrm{d}y \tag{6}$$

**3.2 Mesoscopic Heterogeneity of Ceramics.** For the study of damage and failure of brittle materials, a statistical model of heterogeneous elastic–brittle medium was used [15–17]. The mesoscopic mechanical properties of ceramics are various due to the holes, bubbles, microcracks, and other defects. Assume that the ceramic sheet consists of $N$ mesoscopic units with different

initial tensile strength $\sigma_{Tc}(i)$ and elastic modulus $E(i,0)$, $i=1,\ldots,N$, both of which follow the Weibull statistical distribution function

$$f(\zeta)=\frac{m}{\zeta_0}\left(\frac{\zeta}{\zeta_0}\right)^{m-1}\exp\left[-\left(\frac{\zeta}{\zeta_0}\right)^{m}\right] \tag{7}$$

where $\zeta$ represents the initial tensile strength or elastic modulus of mesoscopic unit; the mean value $\zeta_0$ represents the initial strength and elastic modulus of materials, i.e., $\sigma_{Tc0}$ and $E_0$, respectively; the Weibull modulus $m$ relates to the heterogeneity of materials, that is to say, the smaller the $m$ is, the more diverse the $\sigma_{Tc}(i)$ and $E(i,0)$ are. $\sigma_{Tc}(i)$ and $E(i,0)$ are assigned as follows [21]:

$$\begin{cases} E(i,0)=E_0(-\ln\xi_i)^{1/m} \\ \sigma_{Tc}(i)=\sigma_{Tc0}(-\ln\xi_i)^{1/m}, \quad i=1\ldots N \end{cases} \tag{8}$$

where $\xi_i$ is the pseudouniformly distributed random number in the interval [0,1].

**3.3 Statistical Mesoscopic Damage Mechanics.** For convenience, the complex stress state of the mesoscopic unit is equivalent to a unidirectional stress state, and then, the constitutive relation of a mesoscopic unit can be expressed as

$$\sigma(i,t)=[1-D(i,t)]E(i,0)\varepsilon(i,t) \tag{9}$$

where $\sigma(i,t)$, $\varepsilon(i,t)$, and $D(i,t)$ are the stress, strain, and damage variables of the $i$th mesoscopic unit. $D(i,t)$, ranged from 0 to 1, indicates the damage degree, in which the "health" and "failure" are represented by 0 and 1, respectively. The damage of the mesoscopic unit is reflected by the reduction of its elastic modulus, and the elastic modulus of the $i$th damaged mesoscopic unit can be expressed by

$$E(i,t)=[1-D(i,t)]E(i,0) \tag{10}$$

Furtherly, the tensile, compression, and shear modes are three possible damage modes of the mesoscopic unit subjected to external load, and $D(i,t)$ can be determined by

$$D(i,t)=\max\{D_T(i,t),D_C(i,t),D_S(i,t);D(i,t-\Delta t)\}, \quad \Delta t>0 \tag{11}$$

where $D_T(i,t)$, $D_C(i,t)$, and $D_S(i,t)$ are the damage variables of the $i$th mesoscopic unit under the tensile, compression, and shear modes, respectively. The tensile strain is defined as positive and the compressive strain is defined as negative. The unidirectional-stress-state equivalent expressions of the damage evolution function under the above three damage modes will be introduced as follows.

As the $i$th mesoscopic unit is in the tensile damage mode, the damage evolution equation can be expressed as (Fig. 4(*a*)) [22]

$$D_T(i,t)=\begin{cases} 0 & 0\le\varepsilon_T(i,t)\le\varepsilon_{Tc}(i) \\ \dfrac{\varepsilon_T(i,t)-\varepsilon_{Tc}(i)}{\varepsilon_{Tu}(i)-\varepsilon_{Tc}(i)}\dfrac{\varepsilon_{Tu}(i)}{\varepsilon_T(i,t)} & \varepsilon_{Tc}(i)<\varepsilon_T(i,t)<\varepsilon_{Tu}(i) \\ 1 & \varepsilon_T(i,t)\ge\varepsilon_{Tu}(i) \end{cases} \tag{12}$$

where $\varepsilon_{Tc}(i)=\sigma_{Tc}(i)/E(i,0)$ is the critical tensile strain of the $i$th unit, $\varepsilon_{Tu}(i)$ is assumed to be $\lambda_T\varepsilon_{Tc}(i)$ and the coefficient $\lambda_T>1$, and the equivalent tensile strain $\varepsilon_T(i,t)$ can be expressed by

$$\varepsilon_T(i,t)=\sqrt{\langle\varepsilon_1(i,t)\rangle^2+\langle\varepsilon_2(i,t)\rangle^2+\langle\varepsilon_3(i,t)\rangle^2} \tag{13}$$

where $\varepsilon_1$, $\varepsilon_2$, and $\varepsilon_3$ are three principal strains of the mesoscopic unit, respectively, and the function $\langle\zeta\rangle$ is defined by

$$\langle\zeta\rangle=\begin{cases}\zeta, & \zeta\ge 0\\ 0, & \zeta<0\end{cases} \tag{14}$$

As the $i$th mesoscopic unit is in the compression damage mode, the damage evolution equation can be expressed as (Fig. 4(*b*)) [22]

$$D_C(i,t)=\begin{cases} 0 & -\varepsilon_{Cc}(i)\le\varepsilon_C(i,t)\le 0 \\ \dfrac{\varepsilon_C(i,t)+\varepsilon_{Cc}(i)}{\varepsilon_{Cu}(i)-\varepsilon_{Cc}(i)}\dfrac{\varepsilon_{Cu}(i)}{\varepsilon_C(i,t)} & -\varepsilon_{Cu}(i)<\varepsilon_C(i,t)<-\varepsilon_{Cc}(i) \\ 1 & \varepsilon_C(i,t)\le-\varepsilon_{Cu}(i) \end{cases} \tag{15}$$

where $\varepsilon_{Cc}(i)=\sigma_{Cc}(i)/E(i,0)$ is the critical compressive strain of the $i$th unit, $\sigma_{Cc}(i)$ and $\varepsilon_{Cu}(i)$s are assumed to be $\omega\sigma_{Tc}(i)$ and $\lambda_C\varepsilon_{Cc}(i)$, respectively, and the coefficients $\omega>1$ and $\lambda_C>1$, and the equivalent compressive strain $\varepsilon_C(i,t)$ can be expressed by

$$\varepsilon_C(i,t)=-\sqrt{\langle-\varepsilon_1(i,t)\rangle^2+\langle-\varepsilon_2(i,t)\rangle^2+\langle-\varepsilon_3(i,t)\rangle^2} \tag{16}$$

As the $i$th mesoscopic unit is in the shear damage mode, the damage evolution equation of the mesoscopic unit can be expressed as (Fig. 4(*c*)) [15]

$$D_S(i,t)=\begin{cases} 0 & \varepsilon_{Sc}(i,t)\le\varepsilon_S(i,t)\le 0 \\ 1-\beta\dfrac{\varepsilon_{Sc}(i,t)}{\varepsilon_S(i,t)} & \varepsilon_{Su}(i,t)<\varepsilon_S(i,t)<\varepsilon_{Sc}(i,t) \\ 1 & \varepsilon_S(i,t)\le\varepsilon_{Su}(i,t) \end{cases} \tag{17}$$

Based on the Mohr–Coulomb criterion [23], the critical shear strain of the $i$th unit $\varepsilon_{Sc}(i,t)$ can be deduced by

$$\varepsilon_{Sc}(i,t)=\frac{1}{E(i,0)}\left\{-\frac{2\sin\varphi}{1-\sin\varphi}\sigma_{Tc}(i)+\frac{1+\sin\varphi}{1-\sin\varphi}\sigma_1(i,t)-\nu[\sigma_1(i,t)+\sigma_2(i,t)]\right\} \tag{18}$$

and the equivalent shear strain is equal to

$$\varepsilon_S(i,t)=\varepsilon_3(i,t) \tag{19}$$

where $\varphi$ is the friction angle of the mesoscopic unit; $\nu$ is the Poisson's ratio; $\sigma_1$ and $\sigma_2$ are the first and second principal stresses, respectively; $\varepsilon_3$ is the third principal strain; and $\varepsilon_{Su}(i,t)$ is assumed to be $\lambda_S\varepsilon_{Sc}(i,t)$ and the coefficient $\lambda_S>1$. Assume that the shear strength of the damaged unit $\sigma_r(i,t)=\beta\sigma_{Sc}(i,t)$, in which $\sigma_{Sc}(i,t)=E(i,t)\varepsilon_{Sc}(i,t)$ is the shear strength of the intact unit and $\beta$ is the reduction coefficient that ranges from 0 to 1. Unlike in the case of tensile or compressive damage mode, friction force is generated as the mesoscopic unit subjected to shear stress. Since the friction force is not a constant but relative to the stress state, the shear strength of the mesoscopic unit changes over time.

**3.4 Numerical Simulation for Thermal Shock Process.** In the framework of the above statistic mesoscopic damage mechanics, the ceramic specimen is divided into $N=1000\times200$ mesoscopic units with dimensions of 0.05 mm × 0.05 mm. Each unit is assigned to the same values of Poisson's ratio $\nu$, thermal expansion coefficient $\alpha$, thermal conductivity $k$, constant-pressure specific heat $c$, density $\rho$, frictional angle $\varphi$, and coefficients $\lambda_T=2$, $\lambda_C=2$, $\lambda_S=6$, $\omega=6$, and $\beta=0.5$, but different values of initial tensile strength $\sigma_{Tc}(i)$ and initial elastic modulus $E(i,0)$ due to

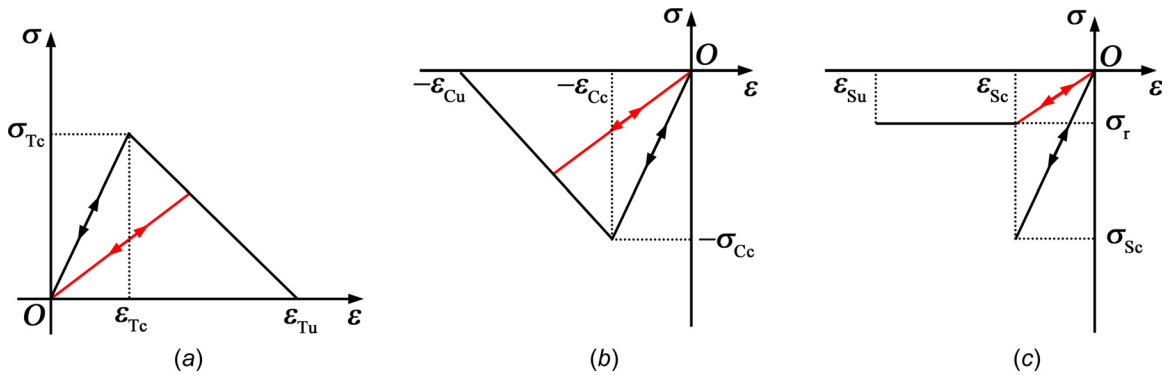


**Fig. 4 Damage constitutive model of the mesoscopic unit: (*a*) tensile mode, (*b*) compressive mode, and (*c*) shear mode**

mesoscopic heterogeneity. Moreover, assume that the above parameters, the initial strength $\sigma_{Tc0}$ and elastic modulus $E_0$ of materials, do not change with the temperature (Table 1). However, the heat transfer coefficient $h$ increases significantly with temperature [24]. For simplicity, the Biot number $\mathrm{Bi} = hH/k$ is taken as 2.5 and 10, respectively, for the quench temperature $T_0 \leq 280\,^{\circ}\mathrm{C}$ and $T_0 > 280\,^{\circ}\mathrm{C}$.

Finite element is adopted to simulate the thermal shock process of ceramic sheet. Each of the mesoscopic unit is characterized by an eight-node thermomechanical coupling element. The time step is 0.001 s. At $t = 0$, all the damage variables of the mesoscopic unit are initialized as zero, and the initial and boundary conditions are imposed according to Eqs. (2) and (3). At time $t$, i.e., the $j$th time step, the temperature and stress fields are solved by ANSYS according to Eqs. (1)–(5), the damage variable of the mesoscopic unit is calculated by Eq. (11), and the elastic modulus of the unit is updated by Eq. (10). At the next $(j+1)$th time step, the stress field is calculated by the updated elastic modulus. In order to avoid the singularity of the stiffness matrix, the elastic modulus of the failure mesoscopic unit is assumed as $10^{-6}$ MPa. Figure 2(*b*) shows the final simulation results of thermal shock cracks, which are composed of the failure mesoscopic units, of three specimens quenched at 400 °C.

## 4 Experimental Verification of the Model Effectiveness

Comparing the simulation results (Fig. 2(*b*)) with the experimental results (Fig. 2(*a*)), it can be seen that both crack patterns present a hierarchical structure of long and shock cracks, and the long cracks separate by the short cracks. Crack depth is defined as the maximum vertical distance from the tip of a crack to the side, and its dimensionless expression was obtained by dividing by half the specimen height (5 mm). Figure 5 shows the statistical distributions of the thermal shock crack depths of six ceramic sheets. Both the experimental and simulation results present a typical bimodal distribution which can be well fitted by the bimodal Gaussian function

**Table 1 Thermal and mechanical parameters of the 99% $Al_2O_3$ ceramic [25]**

| Thermal conductivity $k$ W/(m K) | Constant-pressure specific heat $c$ J/(kg K) | Poisson's ratio $\nu$ |
|---|---|---|
| 31 | 880 | 0.22 |
| Density $\rho$ (kg/m$^3$) | Frictional angle $\varphi$ (deg) | Coefficient of thermal expansion $\alpha$ (K$^{-1}$) |
| 3980 | 30 | $6.8 \times 10^{-6}$ |
| Elastic modulus $E_0$ (GPa) | Tensile strength $\sigma_{Tc0}$ (MPa) | Weibull modulus $m$ |
| 370 | 300 | 5 |

$$f(x) = \sum_{n=1}^{2} \frac{A_n}{w_n\sqrt{\pi/2}} e^{-2\frac{(x-p_n)^2}{w_n^2}} \tag{20}$$

where $p_n$, $w_n$, and $A_n$ are the position, width, and area of the $n$th peak, respectively, and the fitting values are shown in Table 2. The bimodal Gaussian fitting values $p_1$ and $p_1$, which are the mainly concerned here, represent the mean depth of long and short cracks, and their relative errors between the numerical and experimental results are less than 5%.

Moreover, the average crack spacing with respect to the crack length is analyzed statistically to characterize the spatial distribution of multiple cracks. The average crack spacing has been determined by counting the intersection points of cracks with a straight line in the crack length [11]. These values were normalized by the half-specimen height (5 mm) to obtain the corresponding

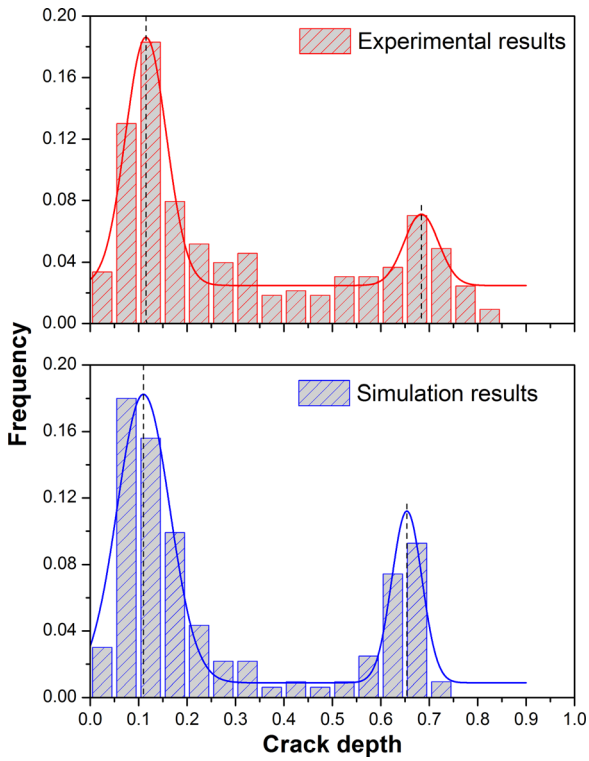


**Fig. 5 Statistic distributions of the thermal shock crack depths of the ceramic sheets. Cracks of six specimens are adopted in the statistical analysis each. The quench and water temperatures are 400 °C and 17 °C, respectively. The solid line represents the bimodal Gaussian fitting function, and the dotted line indicates the positions of the bimodal peak.**

**Table 2 Bimodal Gaussian function fitting parameters**

| | $p_1$ | $p_2$ | $w_1$ | $w_2$ | $A_1$ | $A_2$ |
|---|---|---|---|---|---|---|
| Experimental result | 0.115 | 0.683 | 0.084 | 0.071 | 0.017 | 0.004 |
| Simulation result | 0.110 | 0.654 | 0.108 | 0.061 | 0.024 | 0.008 |

dimensionless values. Figure 6 shows the comparison between the experimental and numerical results on such curves. It is shown that the numerical simulations (solid squares) are close to the real experimental results (hollow circles). As the crack length is smaller which indicates near the specimen boundary, the average crack spacing nearly keeps unchanged. As the crack length increases, the average crack spacing increases gradually which indicates that some cracks are arrested, and the arrested crack must locate between the growth cracks; in other words, the long and shot cracks distribute on each other at intervals.

Therefore, the numerical simulation presents satisfactory agreement with the experimental results. That is to say, the evolution of multiple cracks of the ceramic sheet under water quenching can be effectually simulated by the statistical mesoscopic damage mechanical model.

## 5 Evolution Mechanism of the Multiple Thermal Shock Cracks

**5.1 Evolution Process of Thermal Shock Cracks.** Numerical simulation provides the evolution process of crack patterns of the ceramic sheet under water quenching (Fig. 7). The depths of several long and short cracks of specimen no. 1 versus thermal shock time are shown in Fig. 8. It is observed that the thermal shock crack initiates from the specimen boundary and propagates to the internal along $y$ direction. The evolution has experienced four stages. In the first stage, i.e., $t < t_2$, the initial period of the thermal shock, all cracks grow simultaneously. The cracks initiated almost at the same time on the heat transfer surface and propagated to the inside of the specimen with approximately the same growth rate $6.16 \pm 0.53\,\mathrm{s}^{-1}$ (Fig. 7(*a*)). In the second stage, i.e., $t_2 \le t \le t_{2_{\max}}$, some cracks are arrested one after another until all these cracks arrested. The cracks arrested in this period are called short cracks in the final state, and others continued to extend are long cracks. At $t = t_2 = 0.017\,\mathrm{s}$, the first short crack is arrested while other cracks continue to grow (Fig. 7(*b*)); at $t_2 < t < t_{2_{\max}}$, many short cracks arrested (Fig. 7(*c*)); and at $t = t_{2_{\max}} = 0.030\,\mathrm{s}$, all of the short cracks arrested and the arrested cracks distributed uniformly along the $x$ axis (Fig. 7(*d*)). The black dotted line arrows in Figs. 7(*b*)–7(*d*) indicate the arrested short cracks. In the third stage, i.e., $t_{2_{\max}} < t < t_{3_{\min}}$, all of the long cracks extend simultaneously (white solid line arrows in Fig. 7(*e*)). In the fourth stage, i.e., $t_{3_{\min}} \le t \le t_3$, the long cracks arrested one after another until all of them arrested. The long crack growth rate is $1.49 \pm 0.26\,\mathrm{s}^{-1}$ which is about 1/5 of the first stage. At $t = t_{3_{\min}} = 0.250\,\mathrm{s}$, the first long crack arrested (Fig. 7(*f*)); at $t_{3_{\min}} < t < t_3$, many long cracks arrested (Fig. 7(*g*); and at $t = t_3 = 0.477\,\mathrm{s}$, all of the long cracks arrested and the crack pattern with the alternative distribution of long and short cracks is formed (Fig. 7(*h*)). The pattern at $t = t_3$ be considered as the final state of thermal shock cracks is according to the number of failure mesoscopic units no longer increases as $t > t_3$ (Fig. 9). The white dotted line arrows in Figs. 7(*f*)–7(*h*) indicate the arrested long cracks.

The above mentioned four characteristic moments, $t_2$, $t_{2_{\max}}$, $t_{3_{\min}}$, and $t_3$, represent the moments of the first crack arrested, all of the short cracks arrested, the first long crack arrested, and all of the cracks arrested, respectively. The values obtained from statistical analysis of six specimens are $t_2 = 0.019 \pm 0.001\,\mathrm{s}$, $t_{2_{\max}} = 0.038 \pm 0.004\,\mathrm{s}$, $t_{3_{\min}} = 0.295 \pm 0.027\,\mathrm{s}$, and $t_3 = 0.454 \pm 0.023\,\mathrm{s}$ (Table 3). It can be seen that the crack evolution of the

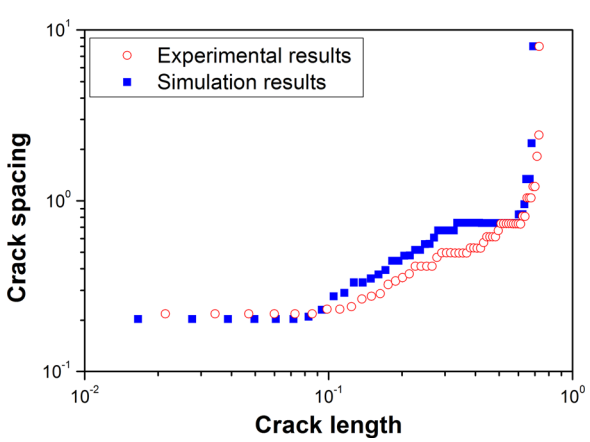


**Fig. 6 Thermal shock crack spacing versus crack length. Hollow circles (○) and solid squares (■) show the experimental and numerical results, respectively.**

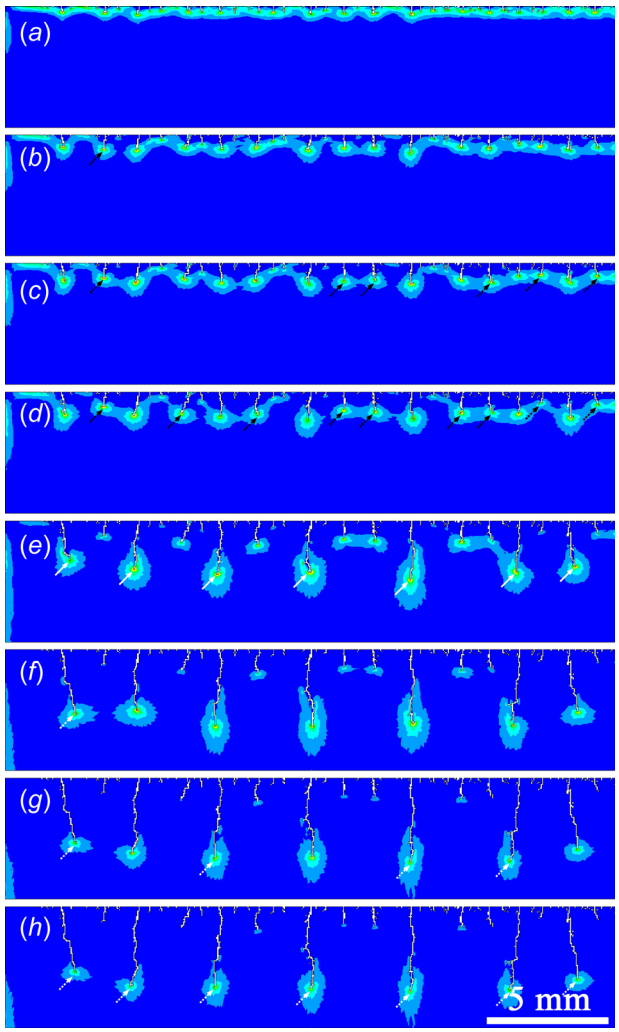


**Fig. 7 Crack evolution process of the ceramic sheet under water quenching by numerical simulations. The upper left 1/4 area of the specimen no. 1 is shown. The quench and water temperature are 400 °C and 17 °C, respectively. White and black arrows represent the long and short cracks, respectively. Dotted and solid lines represent the arrested and extending cracks, respectively. The thermal shock time *t* is (*a*) 0.009 s, (*b*) 0.017 s, (*c*) 0.024 s, (*d*) 0.030 s, (*e*) 0.100 s, (*f*) 0.250 s, (*g*) 0.400 s, and (*h*) 0.477 s, respectively.**

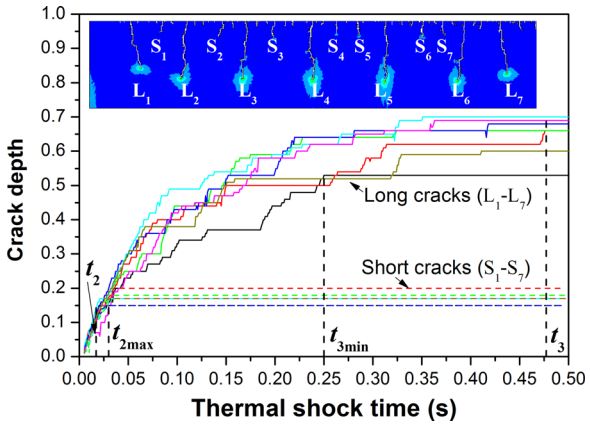


**Fig. 8 Evolution of the crack depth during the whole process of thermal shock. The specimen number is no. 1. Symbols "*L*" and "*S*" represent the long and short cracks, respectively. The short crack has arrested one after the other in the [$t_2$, $t_{2_{max}}$], and the long crack has arrested one by one in the [$t_{3_{min}}$, $t_3$]. $t_2$, $t_{2_{max}}$, $t_{3_{min}}$, and $t_{3_{min}}$ represents the times of the first crack arrested, all short cracks arrested, the first long crack arrested, and all cracks arrested, respectively.**

ceramic sheet under water quenching experienced that all cracks almost initiate simultaneously at the heat exchange surface with an approximately equal growth rate in the initial period of about 0.019 s, the short cracks arrested in succession in 0.019 s, all of the long cracks continue to grow in 0.257 s and then arrested in succession in 0.159 s, and the crack pattern with long and short grading is formed finally.

**5.2 Energy Mechanism of Crack Depth Grading.** After the ceramic sheet is heated to the predetermined temperature and kept for about 20 min, the specimen will reach thermal equilibrium with uniform temperature field and a lot of thermal energy is stored in the specimen. At the moment of the specimen contact the water, heat exchange occurs at the specimen boundary between specimen and water, the temperature field changes rapidly, and the temperature gradient appears. The results of the temperature gradient lead to the difference in thermal expansion between crystals or phases, and the thermal stress will arise [26]. In the process of water quenching, one part of the thermal energy stored in the specimen converted to the elastic strain energy, one part released into the surrounding water by the heat exchange, and the rest is the residual heat energy that not yet be converted or exchanged. In the present study, the elastic strain energy is

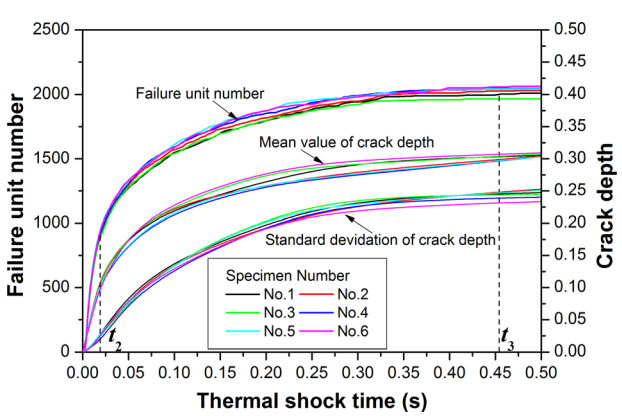


**Fig. 9 Evolution process of the failure unit number and crack depth under thermal shock. $t_2$ and $t_3$ represent the thermal shock times of the first crack arrested and all cracks arrested, respectively.**

**Table 3 Characteristic moments for crack evolution under water quenching**

| Time (s) | No. 1 | No. 2 | No. 3 | No. 4 | No. 5 | No. 6 | Average | Std. |
|---|---|---|---|---|---|---|---|---|
| $t_2$ | 0.017 | 0.020 | 0.018 | 0.021 | 0.017 | 0.019 | 0.019 | 0.001 |
| $t_{2_{max}}$ | 0.030 | 0.038 | 0.039 | 0.037 | 0.040 | 0.041 | 0.038 | 0.004 |
| $t_{3_{min}}$ | 0.250 | 0.339 | 0.293 | 0.286 | 0.290 | 0.313 | 0.295 | 0.027 |
| $t_3$ | 0.477 | 0.473 | 0.420 | 0.463 | 0.423 | 0.468 | 0.454 | 0.023 |

concerned since it directly determines the crack initiation and propagation.

The elastic strain energy stored in the specimen, calculated by Eq. (6), with respect to the thermal shock time is obtained according to the statistical mesoscopic mechanical damage model (Fig. 10 and Table 4). As $t \le t_1$, i.e., in the initial stage of the water quenching, the temperature and stress fields changed suddenly, and the stored elastic strain energy increased rapidly and reached the peak in a short time. As $t_1 < t \le t_2'$, the elastic strain energy decreased gradually due to the generation of a large number of the cracks, that is, the elastic strain energy was released in the form of crack initiation. As $t_2' < t \le t_3$, the elastic strain energy increased gradually first due to some cracks arrest and then decreased.

The above mentioned three characteristic moments, $t_1$, $t_2'$, and $t_3$, represent the moments of the elastic strain energy reached to the first peak and the first minimum value, and all of the cracks arrested, respectively. The values obtained from statistical analysis of six specimens are $t_1 = 0.010 \pm 0.001$ s, $t_2' = 0.028 \pm 0.004$ s, and $t_3 = 0.454 \pm 0.023$ s (Table 4). Compare Tables 3 and 4, it can be seen that $t_2'$ located at the time interval of short crack arrest, i.e., $[t_2, t_{2_{max}}]$.

Thus, it can be seen that the driving force of crack initiation and growth comes from the elastic strain energy stored in the specimen. In the period of $t_1 < t < t_2$, the elastic strain energy decreased due to crack extending, and all cracks grow at almost same velocity. As the elastic strain energy decreased to a certain value at $t = t_2$, just before $t_2'$ which corresponds to the moment of the minimum elastic energy, the first crack arrested and other cracks continued to extend. After that, some cracks arrested one after another, and this caused the gradual increasing of the elastic strain energy after $t_2$ which can continue to drive other cracks extending as $t_2 < t < t_3$, until all cracks arrested at $t = t_3$. During the water quenching process, the elastic strain energy reached a local minimum value, which is closely related to the physical

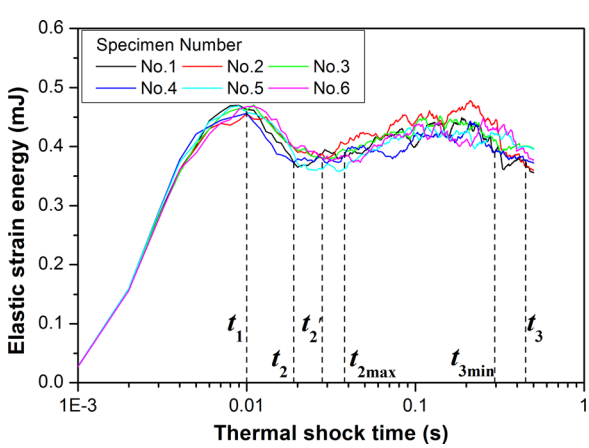


**Fig. 10 Evolution process of the elastic strain energy stored in a specimen during thermal shock. $t_1$ and $t_2'$ represent the times of the first peak and first minimum elastic strain energy, respectively. $t_2$, $t_{2_{max}}$, $t_{3_{min}}$, and $t_{3_{min}}$ represent the times of the first crack arrested, all short cracks arrested, the first long crack arrested, and all cracks arrested, respectively.**

**Table 4 Characteristic moments for the evolution of elastic strain energy under water quenching**

| Time (s) | No. 1 | No. 2 | No. 3 | No. 4 | No. 5 | No. 6 | Average | Std. |
|---|---|---|---|---|---|---|---|---|
| $t_1$ | 0.009 | 0.010 | 0.011 | 0.010 | 0.009 | 0.011 | 0.010 | 0.001 |
| $t_2'$ | 0.020 | 0.030 | 0.031 | 0.030 | 0.025 | 0.031 | 0.028 | 0.004 |
| $t_3$ | 0.477 | 0.473 | 0.420 | 0.463 | 0.423 | 0.468 | 0.454 | 0.023 |

process of the crack arrest. This indicated that the elastic strain energy is the driving agent of the crack growth, and the crack arrest, which eventually leads to the depth grading, is mainly caused by the lack of the elastic strain energy.

**5.3 Stress Analysis of the Crack Depth Grading.** Further statistical analysis on numerical simulations indicates that the depths of the multiple cracks are different during the whole water quenching process, even in the initial stage. The fluctuation of crack depth, i.e., its standard deviation, increases with increasing thermal shock time (Fig. 9). In the initial stage of thermal shock, the fluctuation is mainly due to the mesoscopic heterogeneity of ceramics. However, the interaction between the multiple cracks is the main reason of making the fluctuation strongly amplified and presenting crack depth grading in the end.

A simplified model is introduced to study the crack interaction with existing small fluctuations. Consider a plane stress problem for a homogeneous elastic sheet with 15 parallel cracks of equal spacing along the surfaces $x = \pm H$ perpendicular to the boundaries (Fig. 11). All the 15 cracks have equal depth $p$ in Fig. 11(*a*), while the middle crack no. 8 has depth $p + \Delta p$ and other 14 cracks have depth $p$ in Fig. 11(*b*). The specimen size, initial and boundary conditions, and material parameters are the same as aforementioned (Fig. 3 and Table 1). The crack spacing is assigned as 0.18 since the statistical spacing of our experiments and simulations is 0.174 and 0.177, respectively. Moreover, $p$ and $\Delta p$ are taken as 0.10 and 0.02, respectively, which is corresponding to the crack configuration closing to depth grading just before the moment $t_2$ (Fig. 9). The six-node triangle singular element and eight-node thermomechanical coupling element are adopted near the crack tip and other parts, respectively, in the finite element mesh division. In the whole thermal shock process, assume that the cracks do not propagate.

The difference of the stress intensity factors at the crack tips, $\Delta K_I$, between the two crack configurations is obtained and showed in Fig. 12. As $t$ increased, $\Delta K_I$ of crack no. 8 decreased first and then increased, while the values of other cracks are all reduced (Fig. 12(*a*)). It can be concluded that a little growth of a crack, no. 8, would inhibit its own further growth at the early stage but accelerate later, and inhibit the growth of all the adjacent cracks. Moreover, the variation amplitude of $\Delta K_I$ reduced rapidly with the increasing distance between the crack no. 8 and its neighbors, and the crack interaction had locality with interaction distance

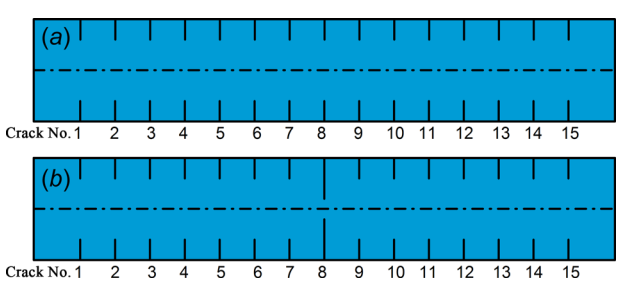


**Fig. 11 Theoretical model of the interaction between multiple cracks with depth fluctuations. (*a*) Cracks with equal depth and spacing and (*b*) cracks with equal spacing and depth except for the middle crack no. 8 with a little more depth.**

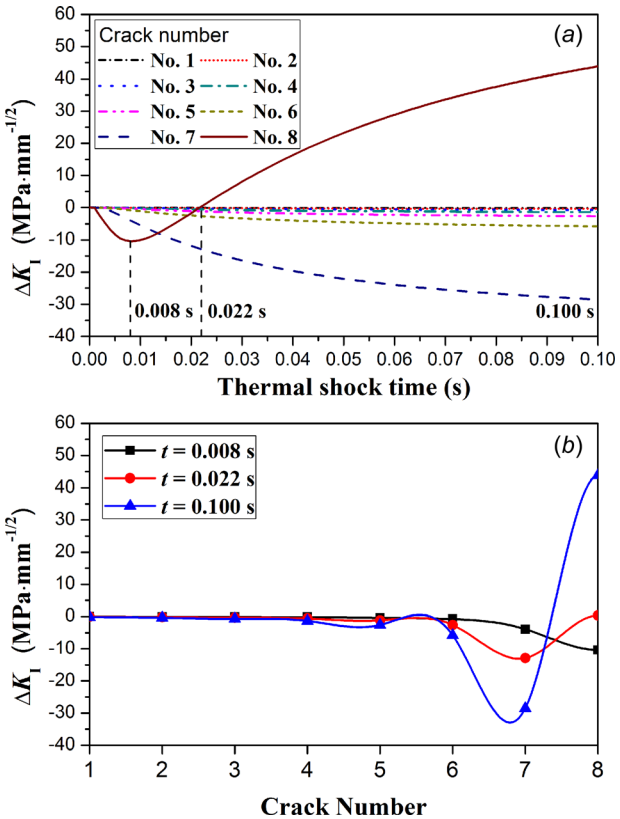


**Fig. 12 Stress intensity factor difference $\Delta K_I$ caused by crack depth fluctuation: (*a*) $\Delta K_I$ versus thermal shock time and (*b*) $\Delta K_I$ versus spatial location of crack. The crack spacing, depth, and depth fluctuation are taken as 0.18, 0.1, and 0.02, respectively, according to the statistical analysis of experimental and numerical results. For symmetry, only eight cracks, nos. 1–8, are shown.**

about 1–2 crack spacing (Fig. 12(*b*)). The interaction modes between the multiple parallel cracks induced by depth fluctuations have common characteristics with different values of the crack parameters, such as spacing, depth, and its fluctuation. Statistical analysis on the experimental and simulation results shows that the thermal shock cracks of ceramic sheet present three depth grading modes, i.e., two long cracks separated by one, two, and three short cracks, and this is mainly caused by the locality of the crack interaction.

Therefore, the evolution of the multiple cracks in the ceramic sheet under the thermal shock has the following characteristics: (1) In the early stage of thermal shock, many cracks have generated on the heat transfer surface almost at the same time and propagate to the interior of the specimen under the drive of elastic strain energy, and the slight depth fluctuations are generated due to the mesoscopic heterogeneity of materials. (2) The interaction between the multiple cracks induced by the depth fluctuations is divided into two stages. In the first stage, once a crack exceeds its adjacent cracks, its crack tip stress intensity factor is reduced, while the adjacent cracks will extend and catch up with this crack, that is, most cracks will extend stably grow and crack depth grading will not appear. In the second stage, the crack stress intensity factor of the relatively longer crack increases gradually, and promotes itself extending, while that of the relatively short crack decreases gradually and inhibits growth even, and the crack pattern of long and short grading will be formed. (3) The crack interaction has locality which reduces rapidly with the distance between two cracks, and it is the interaction locality caused the interval distribution of long and short cracks.

## 6 Multiple Cracks With the Different Quench Temperature

Figures 13 and 14 show the experimental and simulation crack patterns of ceramic sheets under the water quenching at different quench temperature, $T_0$, 220 °C, 240 °C, 260 °C, 280 °C, 290 °C, 300 °C, 400 °C, 500 °C, and 600 °C, respectively. Obviously, the thermal shock cracks present different grading features with different quench temperatures, which is similar to our previous study [27]. This is mainly caused by the locality of the crack interaction. For the thermal shock in the ceramic sheet, the experiment results (Fig. 13) and simulation results (Fig. 14) show that the single peak statistical distribution of the crack depth is translated gradually in to double peak with the increase of the thermal shock temperature, which is mainly due to the interaction between the multiple cracks, as it has local feature decaying rapidly with the increase of crack spacing. At lower quench temperature, i.e., $220\,^{\circ}\mathrm{C} \le T_0 \le 280\,^{\circ}\mathrm{C}$, the crack depth is almost at the same level due to the poor interaction since the crack spacing is much large; each crack can be considered as isolated crack, and the stress state is almost identical during the thermal shock process, and the final depths of these cracks are on the same level. At higher temperature, i.e., $T_0 > 280\,^{\circ}\mathrm{C}$, the interval distribution of the long and short cracks appeared. In this stage, the crack spacing decreases, the interaction between the cracks is strengthened, and eventually crack grading appears.

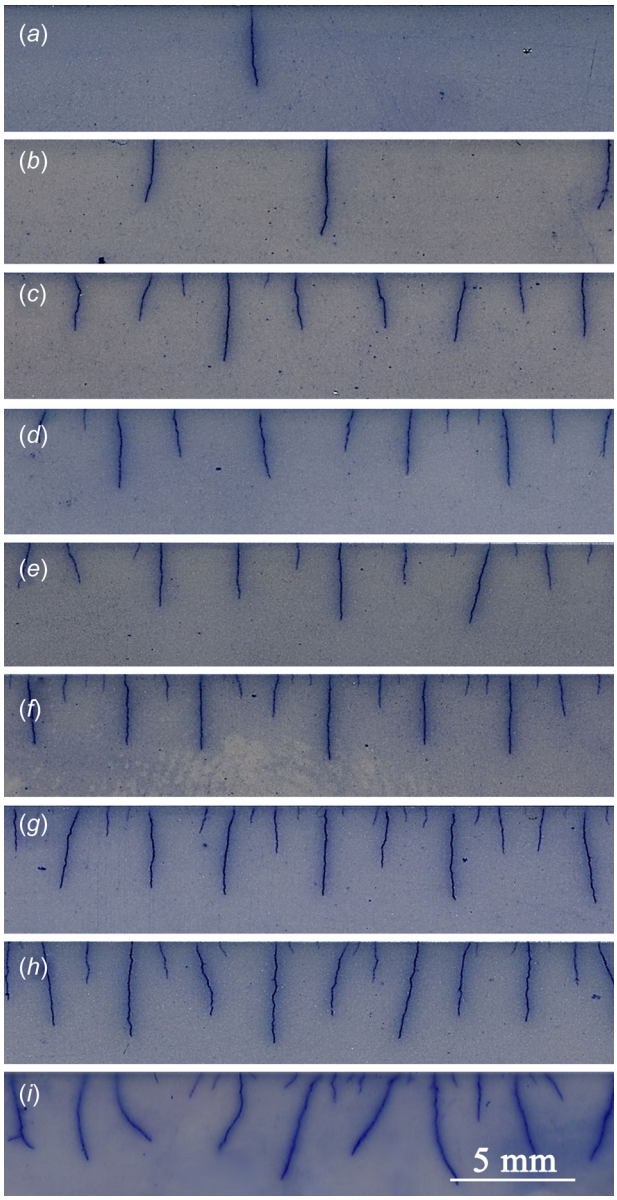


**Fig. 13 Experimental crack patterns of the ceramic sheets under thermal shock. The upper left 1/4 area of the specimen is shown. The water temperature is 17 °C. The quench temperature is (*a*) 220 °C, (*b*) 240 °C, (*c*) 260 °C, (*d*) 280 °C, (*e*) 290 °C, (*f*) 300 °C, (*g*) 400 °C, (*h*) 500 °C, and (*i*) 600 °C, respectively.**

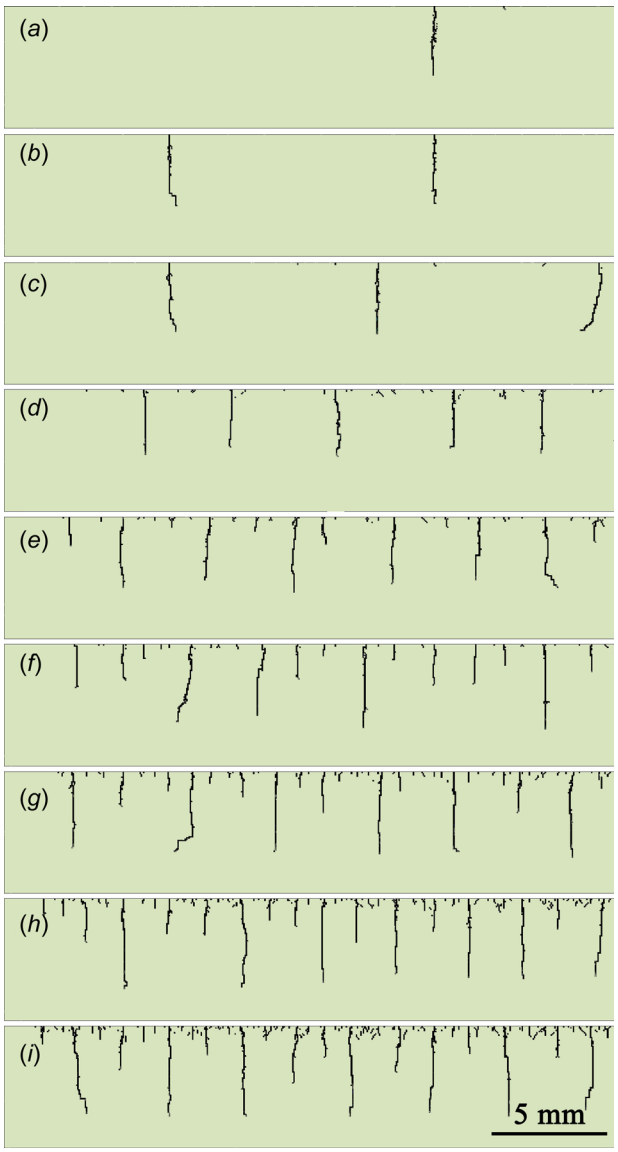


**Fig. 14 Numerical crack patterns of the ceramic sheets under thermal shock. The upper left 1/4 area of the specimen is shown. The water temperature is 17 °C. The quench temperature is (*a*) 220 °C, (*b*) 240 °C, (*c*) 260 °C, (*d*) 280 °C, (*e*) 290 °C, (*f*) 300 °C, (*g*) 400 °C, (*h*) 500 °C, and (*i*) 600 °C, respectively. The water temperature is 17 °C.**

## 7 Conclusion

Based on the statistical mesoscopic mechanics, a model is introduced to study the thermal shock mechanisms of ceramic materials. The distribution of the crack depth and the average crack spacing with respect to the crack length have been analyzed statistically to quantitatively characterize the thermal shock cracks of the ceramic sheets. It can be seen that the numerical simulation presents satisfactory agreement with the experimental results. That is, the evolution of multiple cracks of the ceramic sheet

under water quenching can be effectually simulated by the statistical mesoscopic damage mechanical model.

The crack evolution of the ceramic sheet under water quenching experienced four stages, that is, all cracks almost initiate simultaneously at the heat exchange surface with an approximately equal growth rate, the short cracks arrested on by one, and all of the long cracks continue to extend and then arrested in succession. After that, the crack pattern with long and short grading is formed finally. The mechanism of the multiple cracks propagation of ceramics under the thermal shock has been analyzed from the viewpoint of the evolution of the elastic strain energy and stress intensity factor during the water quenching process. It can be concluded that some cracks will arrest as the elastic strain energy stored in the specimen is insufficient to drive all the crack continue to extend. Moreover, the crack interaction makes the multiple cracks with initial small depth fluctuations present long and short grading in the case of thermal shock. The crack interaction has locality which reduces rapidly with the distance between two cracks, and it is the interaction locality that caused the interval distribution of long and short cracks.

## Acknowledgment

The authors are grateful for the support from the National Natural Science Foundation of China through Grant No. 11272313.

## References

[1] Lu, T. J., and Fleck, N. A., 1998, "The Thermal Shock Resistance of Solids," Acta Mater., **46**(13), pp. 4755–4768.
[2] Bazant, Z. P., Ohtsubo, H., and Aoh, K., 1979, "Stability and Post-Critical Growth of a System of Cooling or Shrinkage Cracks," Int. J. Fract., **15**(5), pp. 443–456.
[3] Nemat-Nasser, S., 1978, "Stability of a System of Interacting Cracks," Int. J. Eng. Sci., **16**(4), pp. 277–285.
[4] Nemat-Nasser, S., Keer, L. M., and Parihar, K. S., 1978, "Unstable Growth of Thermally Induced Interacting Cracks in Brittle Solids," Int. J. Solids Struct., **14**(6), pp. 409–430.
[5] Jagla, E. A., 2002, "Stable Propagation of an Ordered Array of Cracks During Directional Drying," Phys. Rev. E, **65**(4), p. 046147.
[6] Bahr, H.-A., Weiss, H.-J., Bahr, U., Hofmann, M., Fischer, G., Lampenscherf, S., and Balke, H., 2010, "Scaling Behavior of Thermal Shock Crack Patterns and Tunneling Cracks Driven by Cooling or Drying," J. Mech. Phys. Solids, **58**(9), pp. 1411–1421.
[7] Bahr, H. A., Bahr, U., and Petzold, A., 1992, "1-D Deterministic Crack Pattern-Formation as a Growth-Process With Restrictions," Europhys. Lett., **19**(6), pp. 485–490.
[8] Bahr, H. A., Fischer, G., and Weiss, H. J., 1986, "Thermal-Shock Crack Patterns Explained by Single and Multiple Crack-Propagation," J. Mater. Sci., **21**(8), pp. 2716–2720.
[9] Jenkins, D. R., 2005, "Optimal Spacing and Penetration of Cracks in a Shrinking Slab," Phys. Rev. E, **71**(5), p. 056117.
[10] Jiang, C. P., Wu, X. F., Li, J., Song, F., Shao, Y. F., Xu, X. H., and Yan, P., 2012, "A Study of the Mechanism of Formation and Numerical Simulations of Crack Patterns in Ceramics Subjected to Thermal Shock," Acta Mater., **60**(11), pp. 4540–4550.
[11] Li, J., Song, F., and Jiang, C., 2013, "Direct Numerical Simulations on Crack Formation in Ceramic Materials Under Thermal Shock by Using a Non-Local Fracture Model," J. Eur. Ceram. Soc., **33**(13–14), pp. 2677–2687.
[12] Li, J., Song, F., and Jiang, C., 2015, "A Non-Local Approach to Crack Process Modeling in Ceramic Materials Subjected to Thermal Shock," Eng. Fract. Mech., **133**, pp. 85–98.
[13] Bourdin, B., Marigo, J.-J., Maurini, C., and Sicsic, P., 2014, "Morphogenesis and Propagation of Complex Cracks Induced by Thermal Shocks," Phys. Rev. Lett., **112**(1), p. 014301.
[14] Sicsic, P., Mango, J.-J., and Maurini, C., 2014, "Initiation of a Periodic Array of Cracks in the Thermal Shock Problem: A Gradient Damage Modeling," J. Mech. Phys. Solids, **63**, pp. 256–284.
[15] Yang, Y. F., Tang, C. A., and Xia, K. W., 2012, "Study on Crack Curving and Branching Mechanism in Quasi-Brittle Materials Under Dynamic Biaxial Loading," Int. J. Fract., **177**(1), pp. 53–72.
[16] Tang, S., Tang, C. A., Liang, Z., and Qinglei, Y. U., 2008, "Failure Process Analysis of Ceramic Materials Subjected to Thermal Shock," Acta Mater. Compositae Sin., **25**(2), pp. 115–122.
[17] Tang, S. B., Zhang, H., Tang, C. A., and Liu, H. Y., 2016, "Numerical Model for the Cracking Behavior of Heterogeneous Brittle Solids Subjected to Thermal Shock," Int. J. Solids Struct., **80**, pp. 520–531.
[18] Xu, X. H., Ma, S. P., Xia, M. F., Ke, F. J., and Bai, Y. L., 2004, "Damage Evaluation and Damage Localization of Rock," Theor. Appl. Fract. Mech., **42**(2), pp. 131–138.
[19] Rong, F., Wang, H., Xia, M., Ke, F., and Bai, Y., 2006, "Catastrophic Rupture Induced Damage Coalescence in Heterogeneous Brittle Media," Pure Appl. Geophys., **163**(9), pp. 1847–1865.
[20] Bai, Y. L., Xia, M. F., Ke, F. J., and Li, H. L., 2006, *Damage Field Equation and Criterion for Damage Localization*, Springer, Beijing.
[21] Devroye, L., 1986, *Non-Uniform Random Variate Generation*, Springer, New York.
[22] Mazars, J., and Pijaudiercabot, G., 1989, "Continuum Damage Theory—Application to Concrete," J. Eng. Mech., **115**(2), pp. 345–365.
[23] Bai, Y., and Wierzbicki, T., 2009, "Application of Extended Mohr–Coulomb Criterion to Ductile Fracture," Int. J. Fract., **161**(1), pp. 1–20.
[24] Zhou, Z., Song, F., Shao, Y., Meng, S., Jiang, C., and Li, J., 2012, "Characteristics of the Surface Heat Transfer Coefficient for $Al_2O_3$ Ceramic in Water Quench," J. Eur. Ceram. Soc., **32**(12), pp. 3029–3034.
[25] Zhang, Y. L., and Ma, J. P., 2006, *Applicable Ceramic Material Manual*, Chemical Industry Press, Beijing.
[26] Kingery, W. D., 1955, "Factors Affecting Thermal Stress Resistance of Ceramic Materials," J. Am. Ceram. Soc., **38**(1), pp. 3–15.
[27] Xu, X. H., Tian, C., Sheng, S. L., Lin, Z. K., and Song, F., 2014, "Characterization of Thermal-Shock Cracks in Ceramic Bars," Sci. China: Phys., Mech. Astron., **57**(12), pp. 2205–2208.